

# DMAD: Dual Memory Bank for Real-World Anomaly Detection

Jianlong Hu<sup>1,2</sup>, Xu Chen<sup>2</sup>, Zhenye Gan<sup>2</sup>, Jinlong Peng<sup>2</sup>, Shengchuan Zhang<sup>1\*</sup>,  
Jiangning Zhang<sup>2</sup>, Yabiao Wang<sup>2</sup>, Chengjie Wang<sup>2</sup>, Liujuan Cao<sup>1</sup>, and  
Rongrong Ji<sup>1</sup>

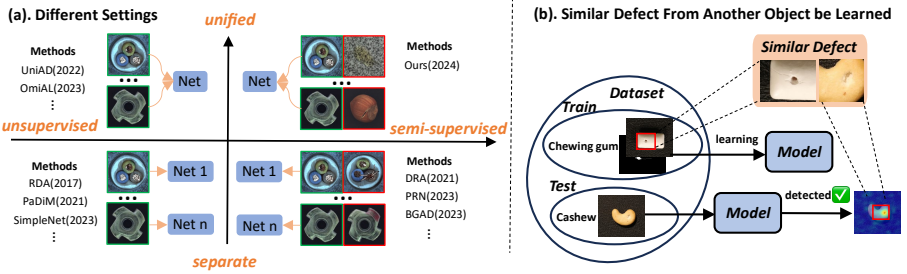
<sup>1</sup> Key Laboratory of Multimedia Trusted Perception and Efficient Computing,  
Ministry of Education of China, School of Informatics, Xiamen University  
<sup>2</sup> YouTu Lab, Tencent

**Abstract.** Training a unified model is considered to be more suitable for practical industrial anomaly detection scenarios due to its generalization ability and storage efficiency. However, this multi-class setting, which exclusively uses normal data, overlooks the few but important accessible annotated anomalies in the real world. To address the challenge of real-world anomaly detection, we propose a new framework named Dual Memory bank enhanced representation learning for Anomaly Detection (DMAD). This framework handles both unsupervised and semi-supervised scenarios in a unified (multi-class) setting. DMAD employs a dual memory bank to calculate feature distance and feature attention between normal and abnormal patterns, thereby encapsulating knowledge about normal and abnormal instances. This knowledge is then used to construct an enhanced representation for anomaly score learning. We evaluated DMAD on the MVTec-AD and VisA datasets. The results show that DMAD surpasses current state-of-the-art methods, highlighting DMAD’s capability in handling the complexities of real-world anomaly detection scenarios. The code will be made available.

**Keywords:** Anomaly Detection · Multi-Class · Dual Memory Bank

## 1 Introduction

Image anomaly detection, also known as surface defect detection, is a process that classifies images into normal and abnormal categories, pinpointing anomalies at the pixel level. Deep learning-based anomaly detection methods have demonstrated superior efficiency compared to manual anomaly localization. Prevailing approaches typically train a unique model for each object, as illustrated in the bottom-left of Figure 1 (a). However, this approach results in increased storage consumption as the number of object categories grows rapidly. To address this issue, UniAD [25] proposed a multi-class setting that leverages all normal data from objects to train a unified model, as depicted in the top-left of Figure 1 (a). Furthermore, under the assumption that anomaly data is unavailable, current anomaly detection methods [6, 14, 23, 31] primarily depend on



**Fig. 1: (a). Comparison of Anomaly Detection’s Settings.** The current research trend is moving from one-class to unified (multi-class) and from unsupervised to semi-supervised, which is more practical. We propose a unified with a few annotated anomalies setting, filling the gap in this field. **(b).** Defects in various objects often exhibit visual similarities. Therefore, defect data from one object can aid the model in detecting similar defects in other objects within a **unified semi-supervised setting**.

unsupervised learning. They explicitly define the boundaries of normal data, as shown on the left of Figure 1 (a). However, these boundaries may lack sufficient accuracy due to the absence of real anomaly data during training, especially when dealing with minor defects. Recent studies [8, 16, 24, 28] have suggested the feasibility of obtaining a handful of anomalies in real-world situations. These semi-supervised approach, shown on the bottom-right of Figure 1 (a), can aid the model in predicting potential anomaly patterns and enhancing its performance. In our proposition, for real-world anomaly detection, training a unified model is more compatible. Furthermore, beyond unsupervised scenarios, semi-supervised scenarios also need to be considered, where a few annotated anomalies are available. We denote this new unified setting with a few annotated anomalies as a **unified semi-supervised setting**, which is illustrated in the top-right of Figure 1 (a). This new setting is filling the research gap.

Under a unified semi-supervised setting, the model utilizes data from all object categories, including normal data, visible abnormal data, and their corresponding supervision information for training. This approach offers several benefits. Firstly, it aligns more closely with real-world scenarios, as there are always some annotated anomalies available for use. Secondly, this setting is more unified and convenient, as all data, including annotations, are utilized by a single model. Thirdly, we observe visually common defects across different object categories, as depicted in Figure 1 (b). By employing this setting for anomaly detection, these similar defects can provide additional advantages during the training process. The challenge of this setting lies in accurately modeling a multi-class distribution while avoiding overfitting to visible anomalies and effectively utilizing the available seen anomalies. To address this, we propose a novel framework: Dual Memory bank enhanced representation learning for Anomaly Detection (DMAD). DMAD is not only suitable for the unified semi-supervised setting, but also compatible with the general unified (multi-class) setting, where no annotated anomalies are available. This makes it well-suited for real-world

anomaly detection, where anomalies may not be initially accessible. However, as the system operates, certain annotated anomalies may emerge for use.

Specifically, DMAD first employs a patch feature encoder to extract the patched feature. To establish a unified decision boundary, a dual memory bank, comprising a normal and abnormal memory bank, is constructed. In the unsupervised scenario, a pseudo abnormal feature set, generated from the feature fusion of normal and outlier features, is utilized as the abnormal memory bank. In semi-supervised scenarios, to mitigate data imbalance, we employ an anomaly center sampling strategy. This strategy expands the abnormal memory bank, supplementing the observed anomalies and the pseudo abnormal feature set. The dual memory bank calculates the distance and cross-attention between patched features and their nearest features in both memory banks, creating a knowledge base for normal and abnormal data. The feature itself, along with its two calculated knowledge components, comprise an enhanced representation. Finally, we use a Multilayer Perceptron (MLP) to learn a mapping between this representation and the anomaly score.

In summary, our contributions are as follows:

1. To address real-world anomaly detection, which encompasses both a general unified setting and a unified semi-supervised setting, we propose a novel dual memory bank-based framework named DMAD. DMAD employs a normal memory bank and a variable abnormal memory bank to handle both scenarios.
2. To effectively utilize the dual memory bank, we introduce a knowledge enhancement module. This module calculates a distance and a cross-attention to form a knowledge representation, facilitating improved anomaly score learning.
3. We conduct extensive experiments on the MVTEC-AD and VisA datasets. The results demonstrate that our model significantly outperforms current state-of-the-art competitors in various settings.

## 2 Related Work

### 2.1 Unsupervised Anomaly Detection

Most anomaly detection methods assume that only normal data can be accessed during training. To this end, various unsupervised techniques are proposed and can be roughly divided into three categories: **1) Reconstruction-based approaches** assume models trained solely on normal samples accurately reconstruct normal regions but struggle with anomalous ones. Initial attempts involve various generative models, including Auto-Encoder [2, 3, 31], Variational Auto-Encoder [7, 13, 29], Generative Adversarial Net [12, 19–21], and Diffusion-based methods [9]. **2) Memory bank-based methods** extract and save representations of normal images from pre-trained deep neural networks and then detect anomalies by comparing the features. SPADE [5] introduces the multi-resolution semantic pyramid anomaly detection framework. PaDiM [6] uses multivariate Gaussian distributions to get a probabilistic representation of the normal class. PatchCore [17] proposes greedy coreset subsampling to lighten the memory bank.

**3) Data augmentation methods** create anomalies on anomaly-free images, transforming anomaly detection into supervised learning [10, 11]. CutPaste [11] introduces a straightforward strategy, cutting an image patch and pasting it randomly onto a larger image. DRÆM [27] employs Perlin noise to generate just-out-of-distribution appearances. NSA [22] integrates Poisson image editing to seamlessly blend scaled patches from different images. SimpleNet [14] introduces Gaussian noise in the feature space, achieving recent state-of-the-art (SOTA) performance. These approaches focus on the problem that no anomalous samples are accessed in training stage. But some challenging anomalies are quite difficult to distinguish due to the lack of true anomalies knowledge.

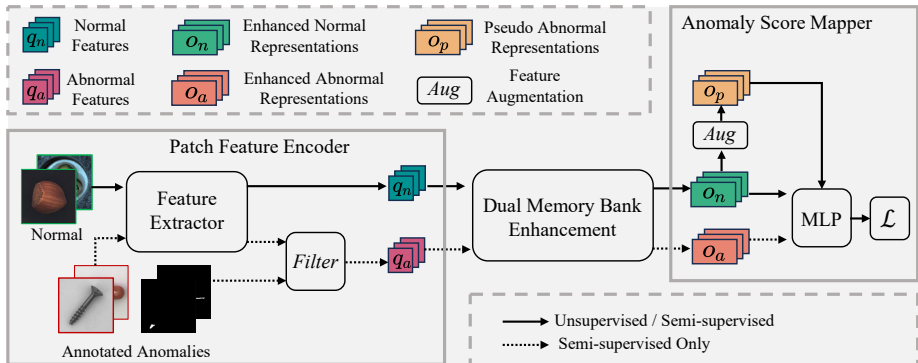
## 2.2 Semi-Supervised Anomaly Detection

In practice, a small amount of anomalous data is obtainable alongside normal data. Some semi-supervised anomaly detection methods aim to fully utilize these scarce but crucial anomalous images. DeepSAD [18] initially focuses on this semi-supervised AD setting and introduces an information-theoretic framework. DRA [8] learns disentangled representations of defects through seen and pseudo anomalies. PRN [28] learns feature residuals between anomalous and normal patterns for accurate detection. BGAD [24] proposes a boundary-guided semi-push-pull contrastive learning mechanism based on conditional normalizing flow.

With the help of anomalous samples, these semi-supervised methods have achieved better results compared to unsupervised methods. However, they are designed for one-class-one-model scenarios, which is cumbersome when the number of product categories increases. Additionally, they are unable to leverage knowledge between different products with similar defects.

## 2.3 Multi-class Unsupervised Anomaly Detection

Most methods propose to train separate models for different classes of objects. However, in real-world application scenarios, the number of intra-class or inter-class may be quite large and separate-trained methods become uncongenial and memory-consuming. Among this, UniAD [25] firstly proposes to detect anomalies from different objects with a unified framework. Meanwhile, UniAD introduces a layer-wise query decoder to the transformer framework to weaken the “identical shortcut” problem of reconstruction-based methods especially in unified setting. OmniAL [30] improves anomaly synthesis, reconstruction, and localization by using panel-guided synthetic anomaly data. These methods are convenient in practical applications because they use a unified model that can cover all objects. However, they cannot utilize defects to enhance their performance. In this paper, we propose DMAD which can model a multi-class distribution and effectively utilize the available anomalies as well.



**Fig. 2: Overview of DMAD.** DMAD is a unified framework that accommodates both unsupervised and semi-supervised scenarios. During training, normal images and seen annotated anomalies are input into the Feature Extractor to obtain patched features. For the anomalies, a *Filter* is utilized to isolate the anomalous parts. Subsequently, a Dual Memory Bank Knowledge Enhancement is employed to obtain enhanced representations of both normal and abnormal. A more detailed illustration is depicted in Figure 3. A pseudo abnormal representation is generated by utilizing a feature augmentation [14]. Ultimately, these normal representations, abnormal representations, and pseudo abnormal representations are used to train a MLP.

### 3 Methodology

**Problem Statement.** In practical industrial scenarios, training a unified model is viewed as more compatible and storage-efficient. The unified anomaly detection system is confronted with two situations simultaneously: a general unified (multi-class) setting [25] and an unified setting with a few annotated anomalies, which can be referred to as unified semi-supervised setting. This dual situation arises depending on the availability of anomalies. In the general unified setting, the model’s training set is denoted as  $\mathcal{X}_{\text{train}} = \{\mathcal{X}_n^i\}_{i=1}^M$ . Here,  $M$  represents the number of objects in the dataset, while  $\mathcal{X}_n$  signifies the normal data. When some annotated anomalies become available, the setting transitions to unified semi-supervised, and the training set changes to  $\mathcal{X}_{\text{train}} = \{\mathcal{X}_n^i\}_{i=1}^M \cup \{\mathcal{X}_{a_s}^i\}_{i=1}^M$ .  $\mathcal{X}_{a_s}$  represents the seen annotated anomalies. The objective is to train a unified neural network, denoted as  $m : \mathcal{X} \rightarrow \mathbb{R}$ , capable of assigning higher anomaly scores to anomalies than to normal instances. For real-world anomaly detection, the model needs to accommodate both settings.

**Overview.** We propose a novel framework, named Dual Memory bank enhanced representation learning for Anomaly Detection (DMAD), designed to tackle the challenges of real-world anomaly detection. DMAD is a unified model that not only utilizes normal data for training but also effectively employs accessible anomalies. An overview of DMAD can be found in Figure 2. DMAD primarily consists of three components: the Patch Feature Encoder (Section 3.1), Dual Memory Bank-based Knowledge Enhancement (Section 3.2), and Anomaly Score

Mapper (Section 3.3). We will subsequently provide a detailed introduction to these three components.

### 3.1 Patch Feature Encoder

The Patch Feature Encoder consists of a Feature Extractor  $F_\Phi : x \rightarrow q$ , and an optional feature filter operation *Filter*. The Feature Extractor  $F_\Phi$  is employed to extract the patched features from an image, which includes a pre-trained backbone and an aggregation operation [17]. The training image is represented as  $x \in \mathbb{R}^{3 \times H \times W}$ , and the patched feature denoted as  $q \in \mathbb{R}^{N \times C}$ . Here,  $N = H_0 \times W_0$  represents the number of patches,  $H_0$  and  $W_0$  denote the height and width of the feature respectively, and  $C$  signifies the feature’s channel.

For a general unified setting, where there are only normal data can be used, for each normal image  $x_n$ , we directly obtain its patched feature  $q_n$ :

$$q_n = F_\Phi(x_n) \quad (1)$$

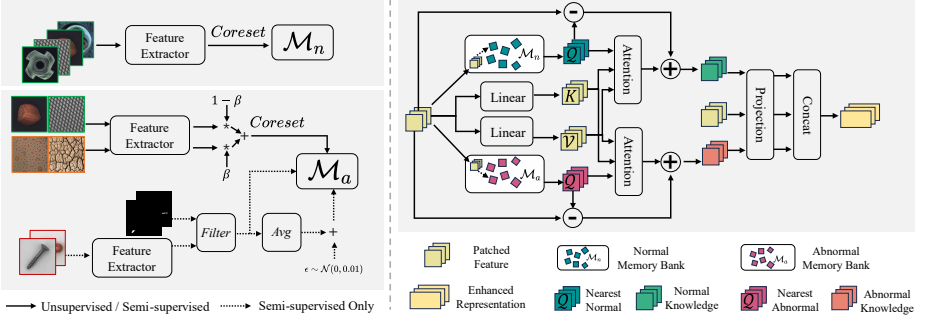
As the detection system runs, some annotated anomalies become accessible and can be incorporated into the training of DMAD. For each seen anomaly  $x_{a_s}$ , we additionally employ a *Filter* operation to isolate the anomalous parts from its extracted patch features  $F_\Phi(x_{a_s})$ . *Filter* is adopted because we have observed that image defects generally constitute a small portion of the image, which needs to be filtered out. We conducted ablation experiments in Section 4.5 to illustrate the importance of the *Filter*. More specifically, we denoted the annotation of a defective image as  $y \in \{0, 1\}^{1 \times H \times W}$ . If the position  $(h, w)$  in the image is normal,  $y(h, w) = 0$ ; otherwise,  $y(h, w) = 1$ . We initially use bilinear interpolation to scale  $y$  to match the resolution of the feature, and then filtered out the corresponding anomalous parts. Therefore, for each defective image  $x_a$ , we could calculate its anomalous patch feature  $q_a \in \mathbb{R}^{N_f \times C}$ :

$$q_a = \text{Filter}(F_\Phi(x_{a_s}), y) \quad (2)$$

Here,  $N_f$  represents the number of anomalous patches, and  $N_f \ll N$ . The patch features will subsequently be enhanced by dual memory bank.

### 3.2 Dual Memory Bank-based Knowledge Enhancement

To learn a comprehensive, unified decision boundary, it is more effective for the model to consider the entire training set, taking into account all different objects simultaneously. Therefore, we employ a dual memory bank  $\mathcal{M}_D$  to introduce additional useful knowledge for anomaly detection.  $\mathcal{M}_D$  comprises a normal memory bank, denoted as  $\mathcal{M}_n$ , which stores normal patterns, and an abnormal memory bank, denoted as  $\mathcal{M}_a$ , which stores all potential defect patterns. First, we will introduce the construction of the  $\mathcal{M}_D$  (Figure 3. Left). Following this, we will explain how to utilize  $\mathcal{M}_D$  to extract additional knowledge, and subsequently use this knowledge to acquire an enhanced representation (Figure 3. Right).



**Fig. 3:** An intuitive illustration of the Dual Memory Bank’s construction is depicted on the **left**. A schematic diagram of the Knowledge Enhancement based on the Dual Memory Bank is shown on the **right**. DMAD uses the Dual Memory Bank to create an enhanced representation encompassing normal and abnormal knowledge.

**Dual Memory Bank Construction.** To construct  $\mathcal{M}_n$ , the patched features of all normal data  $\{\mathcal{X}_n^i\}_{i=1}^M$  are extracted and then processed using a coreset sampling algorithm *Coreset* to retain 2% of them:

$$\mathcal{M}_n = \text{Coreset}\left(\bigcup_{x_n \in \{\mathcal{X}_n^i\}_{i=1}^M} F_{\Phi}(x_n)\right) \quad (3)$$

The construction of  $\mathcal{M}_a$  is tailored to the specific experimental setting. For a general unified setting, annotated anomalies are not available. To address this, we introduce randomly sampled outlier data  $x_o \in \mathbb{R}^{3 \times H \times W}$  from DTD [4] dataset  $\mathcal{X}_o$  to construct the  $\mathcal{M}_a$ , the ablation study presented in Section 4.5 demonstrates the benefits of this. DTD dataset contains diverse textures, amalgamated with the normal data is an efficient strategy to construct the pseudo anomalies. More specifically, we use a  $\beta$  parameter to fuse  $x_o$  with a randomly sampled normal image  $x_n$  at the feature-level, thereby creating the possible defects set  $\mathcal{M}_o$ :

$$\mathcal{M}_o = \text{Coreset}\left(\bigcup_{x_o \in \mathcal{X}_o, x_n \in \{\mathcal{X}_n^i\}_{i=1}^M} (\beta F_{\Phi}(x_o) + (1 - \beta) F_{\Phi}(x_n))\right) \quad (4)$$

In this context, we simply set  $\beta = 0.6$ . In a general unified setting,  $\mathcal{M}_a$  is essentially  $\mathcal{M}_o$ . Once annotated anomalies  $\{\mathcal{X}_{a_s}^i\}_{i=1}^M$  become available, we are able to compute the filtered anomalous patch feature set of observed annotated anomalies, denoted as  $\mathcal{M}_{a_s}$ :

$$\mathcal{M}_{a_s} = \bigcup_{x_{a_s} \in \{\mathcal{X}_{a_s}^i\}_{i=1}^M, y \in \mathcal{Y}} \text{Filter}(F_{\Phi}(x_{a_s}), y) \quad (5)$$

Given the extreme data imbalance between normal and abnormal instances, training the model presents a significant challenge. Based on an intuitively assumption, that in a well-trained embedding space, the data points surrounding the abnormal feature are also likely to be abnormal. Thus we propose the

**Anomaly Center Sampling** strategy, that is adding a small perturbation  $\epsilon \sim \mathcal{N}(0, 0.01)$  to the calculated average abnormal feature  $q_a^{\text{avg}} \in \mathbb{R}^{N \times C}$  to generate pseudo abnormal features set  $\mathcal{M}_p$ .

For the unified semi-supervised setting, the abnormal memory bank is actually a union of  $\mathcal{M}_o$ ,  $\mathcal{M}_{a_s}$  and  $\mathcal{M}_p$ . Once the  $\mathcal{M}_n$  and  $\mathcal{M}_a$  constructed, they are saved on the disk and will unchanged.

**Knowledge Enhancement.** Under a general unified setting, for each patched normal feature  $q_n$  that we obtain from Equation (1), we identify its nearest neighbour from  $\mathcal{M}_n$  and  $\mathcal{M}_a$  respectively, denoted as  $q_{n\cdot n}$  and  $q_{n\cdot a}$ :

$$\begin{aligned} q_{n\cdot n} &= \arg \min_{q^* \in \mathcal{M}_n} \|q_n - q^*\| \\ q_{n\cdot a} &= \arg \min_{q^* \in \mathcal{M}_a} \|q_n - q^*\| \end{aligned} \quad (6)$$

Subsequently, we compute a distance *dist* between the feature and its two nearest neighbour features, denoted as  $d_{n\cdot n}$  and  $d_{n\cdot a}$  separately:

$$\begin{aligned} d_{n\cdot n} &= q_n - q_{n\cdot n} \\ d_{n\cdot a} &= q_n - q_{n\cdot a} \end{aligned} \quad (7)$$

Moreover, we further utilize cross-attention to calculate the attention between the feature and its two nearest neighbour features. We consider the two nearest neighbour features  $q_{n\cdot n}$  and  $q_{n\cdot a}$  as the query embedding  $\mathcal{Q}_n$  and  $\mathcal{Q}_a$ , and use a linear layer to embed the  $q_n$  into key  $\mathcal{K}_n \in \mathbb{R}^{N \times C}$  and value  $\mathcal{V}_n \in \mathbb{R}^{N \times C}$ . The two attention matrix *Attn* is calculated as:

$$\begin{aligned} \mathcal{A}_n &= \text{softmax}(\mathcal{Q}_n(\mathcal{K}_n)^T \mathcal{V}_n) \\ \mathcal{A}_a &= \text{softmax}(\mathcal{Q}_a(\mathcal{K}_n)^T \mathcal{V}_n) \end{aligned} \quad (8)$$

Hence, the knowledge  $k \in \mathbb{R}^{N \times C}$  derived from the dual memory bank is denoted as the addition of *dist* and *Attn*:

$$\begin{aligned} k_{n\cdot n} &= d_{n\cdot n} + \mathcal{A}_n \\ k_{n\cdot a} &= d_{n\cdot a} + \mathcal{A}_a \end{aligned} \quad (9)$$

Both the distance and the attention matrix encapsulate the knowledge about the normality or abnormality of the feature. When scenarios transitions to unified semi-supervised setting, that is the anomalies is accessible, we perform the same operation to calculate the necessary knowledge  $k_{a\cdot n}$  and  $k_{a\cdot a}$  of the anomalous feature  $q_a$  of each seen anomaly  $x_{a_s}$ . It's important to note that in unified semi-supervised setting, the attention matrix is not utilized. This is because we discovered that calculating distances independently yields superior results. The ablation study of this part is shown in Table 4.

After acquiring the knowledge, a projection layer  $\mathcal{P}_\theta$  is applied to the feature and two parts of knowledge. Subsequently, the feature itself with two parts of knowledge are combined to form enhanced normal representation  $o_n \in \mathbb{R}^{N \times 3C}$ :



$$o_n = \text{Cat}(\mathcal{P}_\theta(q_n), \mathcal{P}_\theta(k_{n-n}), \mathcal{P}_\theta(k_{n-a})) \quad (10)$$

*Cat* denotes the concatenation operation. For unified semi-supervised scenarios, we also have enhanced abnormal representation  $o_a \in \mathbb{R}^{N_f \times 3C}$ :

$$o_a = \text{Cat}(\mathcal{P}_\theta(q_a), \mathcal{P}_\theta(k_{a-n}), \mathcal{P}_\theta(k_{a-a})) \quad (11)$$

### 3.3 Anomaly Score Mapper

We employ a MLP, denoted as  $\Psi$ , to learn a mapping between our constructed enhanced representation  $o$ , and the anomaly score  $S \in \mathbb{R}^{H_o \times W_o}$ . A hinge loss function is utilized to optimize the network. In a general unified (multi-class) scenarios, where no negative samples are available, we adopt a feature augmentation strategy [14]. This strategy involves using a Gaussian noise generator to create pseudo negative samples  $o_p \in \mathbb{R}^{N \times 3C}$ . When annotated anomalies are accessible, a three parts hinge loss is used for the model’s optimization:

$$\begin{aligned} \mathcal{L} = & \max(0, 0.5 - \Psi(o_n)) \\ & + \lambda_1 \max(0, 0.5 + \Psi(o_p)) \\ & + \lambda_2 \max(0, 0.5 + \Psi(o_a)). \end{aligned} \quad (12)$$

In the general unified setting,  $\lambda_1 = 1, \lambda_2 = 0$ , while in the unified semi-supervised setting,  $\lambda_1 = 0.5, \lambda_2 = 15$ .

### 3.4 Anomaly Detection and Localization

Given a test image  $x_{\text{test}}$ , we can utilize a well-trained DMAD to derive its patch-level anomaly scores  $S_{\text{test}}$ . We adopt the average of the top-5 anomaly scores as its image-level score. For the pixel-level score, we initially apply bilinear interpolation to  $S_{\text{test}}$ , follow up with a Gaussian smoothing to refine its values.

## 4 Experiments

### 4.1 Datasets and Evaluation Metrics

**MVTec-AD.** MVTEC-AD [1], a widely recognized anomaly detection benchmark, encompasses a diverse dataset of 5,354 high-resolution images from various domains. This dataset is categorized into 5 types of textures and 10 types of objects. The data is divided into training and testing sets, with the training set containing 3,629 anomaly-free images, ensuring a focus on normal samples. On the other hand, the test set consists of 1,725 images, providing a mix of both normal and abnormal samples for comprehensive evaluation. To aid in the anomaly localization evaluation, pixel-level annotations are provided.

**VisA.** The VisA [32] dataset comprises 10,821 high-resolution images, including 9,621 normal images and 1,200 anomaly images. This dataset is organized into

**Table 1:** Image-level AUROC/AP results on the MVTec-AD and VisA datasets for both unsupervised and semi-supervised scenarios under a unified (multi-class) setting.

Datasets	Unsupervised			1 Anomaly			5 Anomalies			10 Anomalies		
	UniAD [25]	SimpleNet* [14]	DMAD	DRA* [8]	BGAD* [24]	DMAD	DRA* [8]	BGAD* [24]	DMAD	DRA* [8]	BGAD* [24]	DMAD
Carpet	99.8 / 99.8	93.6 / 98.1	93.7 / 98.1	98.3 / 98.3	99.2 / 99.6	99.0 / 99.7	99.2 / 99.8	99.5 / 99.8	99.1 / 99.7	98.4 / 99.5	99.6 / 99.7	98.5 / 99.5
Grid	98.2 / 97.5	97.9 / 99.4	96.8 / 99.0	90.4 / 93.4	96.6 / 97.2	97.5 / 99.2	96.2 / 98.7	97.6 / 98.8	98.1 / 99.4	83.6 / 93.5	98.1 / 97.2	99.5 / 99.8
Leather	100 / 100	100 / 100	100 / 100	98.4 / 99.3	100 / 100	100 / 100	98.9 / 99.7	100 / 100	100 / 100	100 / 100	100 / 100	100 / 100
Tile	99.3 / 99.7	99.5 / 99.8	100 / 100	95.5 / 98.1	99.9 / 100	100 / 100	97.2 / 99.1	100 / 100	100 / 100	98.0 / 99.2	100 / 100	100 / 100
Wood	98.3 / 99.5	99.5 / 99.8	99.7 / 99.9	98.1 / 99.5	96.3 / 97.5	99.4 / 99.8	99.8 / 99.9	98.3 / 99.3	99.8 / 99.9	99.5 / 99.8	99.0 / 99.5	99.3 / 99.8
Bottle	99.7 / 100	100 / 100	100 / 100	100 / 99.6	99.8 / 99.7	100 / 100	99.7 / 99.9	100 / 100	100 / 100	99.2 / 99.7	100 / 100	100 / 100
Capsule	96.9 / 96.7	84.2 / 96.5	89.8 / 97.8	72.0 / 95.0	87.6 / 94.3	93.7 / 98.7	73.4 / 91.6	91.4 / 96.8	96.1 / 99.2	80.1 / 86.8	93.4 / 97.0	97.9 / 99.6
Pill	93.7 / 98.6	88.9 / 97.7	91.8 / 98.5	73.6 / 91.4	83.2 / 94.7	93.2 / 98.6	79.3 / 95.7	87.4 / 96.7	92.9 / 99.1	76.4 / 94.9	92.3 / 97.7	94.0 / 98.8
Transistor	99.8 / 99.2	96.4 / 95.6	98.8 / 98.2	64.4 / 62.8	93.0 / 88.3	98.6 / 98.0	64.7 / 53.4	99.2 / 96.9	99.6 / 99.3	66.3 / 60.7	98.2 / 96.6	99.8 / 99.6
Zipper	95.8 / 98.3	99.6 / 99.9	99.5 / 99.9	95.7 / 96.0	98.2 / 99.5	99.7 / 99.9	99.6 / 99.1	99.6 / 99.9	99.4 / 99.8	98.1 / 99.5	99.9 / 100	100 / 100
Cable	95.2 / 95.6	98.1 / 98.8	99.0 / 99.4	74.2 / 92.3	93.1 / 92.1	98.4 / 99.1	89.9 / 94.0	93.1 / 94.4	98.3 / 98.9	80.1 / 88.9	97.1 / 95.7	99.7 / 99.8
Hazelnut	99.8 / 99.9	99.9 / 99.9	100 / 100	95.0 / 97.9	100 / 99.8	100 / 100	89.9 / 95.4	100 / 99.9	100 / 100	98.7 / 99.3	99.8 / 99.7	100 / 100
Metal_Nut	99.2 / 99.7	98.1 / 99.5	99.0 / 99.8	92.0 / 98.0	99.3 / 99.2	99.4 / 99.9	98.5 / 99.6	99.3 / 99.7	100 / 100	97.7 / 99.4	99.1 / 99.5	99.3 / 99.8
Screw	87.5 / 94.9	77.2 / 91.6	84.1 / 93.7	76.7 / 94.6	84.5 / 92.8	93.2 / 96.3	87.0 / 95.4	88.1 / 91.5	92.9 / 97.5	90.9 / 94.9	84.2 / 92.1	97.3 / 99.0
Toothbrush	94.2 / 96.6	89.7 / 95.4	91.7 / 96.4	69.0 / 90.7	96.0 / 97.8	92.5 / 96.8	78.0 / 88.3	99.0 / 97.9	95.7 / 98.0	75.4 / 87.4	96.7 / 96.9	99.2 / 99.5
MVTEC-AD	96.5 / 98.4	94.8 / 98.1	96.3 / 98.7	86.2 / 93.8	95.1 / 96.8	97.4 / 99.1	89.9 / 99.1	96.8 / 98.1	98.3 / 99.4	88.4 / 93.6	97.1 / 98.1	99.0 / 99.7
Candle	85.4 / 20.3	94.1 / 82.5	95.6 / 84.1	92.2 / 69.7	94.6 / 68.8	94.6 / 84.9	90.2 / 69.6	97.3 / 88.8	97.7 / 90.1	90.5 / 63.6	97.5 / 85.3	98.3 / 92.4
Capsules	57.3 / 15.3	68.5 / 35.2	72.8 / 39.8	60.1 / 22.3	71.3 / 33.0	71.7 / 40.5	77.5 / 37.1	76.0 / 56.2	79.0 / 53.9	76.4 / 35.9	80.9 / 63.5	79.4 / 58.0
Cashew	88.7 / 58.2	93.6 / 81.0	93.8 / 81.9	95.7 / 86.1	96.3 / 84.8	95.7 / 87.4	96.2 / 85.6	94.1 / 85.8	95.1 / 85.6	97.4 / 91.1	94.4 / 84.5	96.9 / 90.7
Chewinggum	97.8 / 93.3	97.0 / 95.9	97.1 / 95.2	93.6 / 88.9	98.9 / 96.4	98.3 / 96.7	96.4 / 92.9	98.9 / 96.6	98.1 / 96.9	96.4 / 94.1	99.0 / 97.6	98.7 / 97.6
Fryum	81.3 / 43.3	87.3 / 76.2	90.9 / 78.6	77.5 / 63.0	90.3 / 72.3	92.8 / 83.4	90.5 / 75.4	93.7 / 85.1	93.4 / 83.0	88.4 / 73.6	93.3 / 80.3	96.5 / 89.6
Macaroni1	77.1 / 15.8	87.3 / 46.6	86.9 / 55.9	69.2 / 26.0	90.0 / 53.4	87.2 / 56.8	83.1 / 73.5	96.0 / 77.4	93.7 / 75.1	91.0 / 67.1	94.7 / 74.8	97.3 / 87.4
Macaroni2	72.4 / 15.0	69.5 / 22.8	72.6 / 24.8	53.5 / 11.2	74.9 / 20.7	73.7 / 31.7	82.0 / 57.0	82.4 / 37.0	78.8 / 37.4	83.4 / 61.4	85.2 / 45.7	85.4 / 37.5
Pcb1	90.3 / 45.9	95.6 / 78.5	94.9 / 77.0	87.1 / 54.8	89.8 / 47.5	95.1 / 77.7	70.7 / 48.6	92.2 / 56.1	97.7 / 86.7	83.3 / 52.2	94.3 / 67.9	98.8 / 91.8
Pcb2	87.1 / 48.2	93.8 / 79.7	94.1 / 77.5	85.8 / 49.0	84.7 / 56.9	97.5 / 87.8	83.5 / 51.9	88.9 / 61.1	98.2 / 90.7	75.6 / 23.4	92.7 / 75.0	98.5 / 92.5
Pcb3	80.1 / 30.5	84.9 / 58.2	87.4 / 62.4	77.1 / 24.6	89.7 / 58.0	89.9 / 69.5	68.4 / 22.6	92.3 / 68.8	90.7 / 71.0	72.8 / 17.9	93.7 / 76.2	91.7 / 71.3
Pcb4	91.7 / 68.1	97.9 / 91.2	98.5 / 90.3	75.4 / 33.7	97.1 / 74.9	99.0 / 94.6	86.7 / 74.6	98.8 / 87.2	98.7 / 95.4	80.7 / 63.8	99.3 / 92.2	99.7 / 97.0
Pipe_Fryum	91.2 / 61.4	91.0 / 79.9	91.6 / 79.9	92.1 / 83.1	98.5 / 95.7	95.7 / 85.7	98.7 / 94.3	97.2 / 93.1	96.1 / 91.7	97.6 / 93.2	98.9 / 94.8	98.1 / 93.2
VisA	83.9 / 42.9	88.0 / 69.0	89.7 / 70.5	80.0 / 51.0	89.7 / 63.5	90.9 / 74.7	86.9 / 65.2	92.3 / 74.3	93.1 / 79.8	86.1 / 61.4	93.7 / 78.2	94.9 / 84.9

12 unique object classes. These 12 object classes can be further categorized into three distinct object types: Complex Structures, Multiple Instances, and Single Instances. For our study, we specifically utilized the **2-class few-shot** setting split of the VisA dataset, where both the training and testing sets contain normal and anomalous samples.

**Evaluation Metrics.** We utilize a comprehensive suite of standard evaluation metrics, which includes the Area Under the Receiver Operating Characteristic Curve (AUROC), Average Precision (AP), and the maximum F1-score (F1max). Additionally, for anomaly localization, we employ the Per-Region-Overlap (PRO) metric.

**Table 2:** Results of F1max and PRO comparison on VisA datasets.

	Unsupervised			10 Anomalies		
	UniAD [25]	SimpleNet* [14]	DMAD	BGAD* [24]	DMAD	
F1max-Det	47.3	66.9	<b>67.5</b>	72.3	<b>79.7</b>	
F1max-Loc	28.4	36.3	<b>36.7</b>	<b>47.5</b>	44.9	
PRO	83.0	85.6	<b>85.7</b>	91.9	<b>92.9</b>	

## 4.2 Implementation Details

We utilize the WideResnet50 [26] as our pre-trained CNN backbone, extracting features from both the layer-2 and layer-3 to aggregate into a patched feature [17]. The dimension of this feature is 1536. For the projection layer, we employ a single fully connected layer to project the features and knowledge. The MLP consists of four nonlinear layers, each of which includes a linear layer, batch normalization, and leaky ReLU activation. Skip connections are applied between

**Table 3:** Pixel-level AUROC/AP results on the MVTec-AD and VisA datasets for both unsupervised and semi-supervised scenarios under a unified (multi-class) setting.

Datasets	Unsupervised			1 Anomaly		5 Anomalies		10 Anomalies	
	UniAD [25]	SimpleNet* [14]	DMAD	BGAD* [24]	DMAD	BGAD* [24]	DMAD	BGAD* [24]	DMAD
Carpet	<b>98.5 / 51.7</b>	96.5 / 38.4	97.5 / 42.3	<b>99.2 / 69.1</b>	98.8 / 60.8	<b>99.4 / 72.1</b>	99.1 / 71.0	<b>99.4 / 75.1</b>	99.1 / 72.3
Grid	96.5 / 22.5	96.2 / 22.6	<b>97.2 / 26.0</b>	<b>98.6 / 39.6</b>	97.1 / 30.4	<b>98.9 / 40.3</b>	96.9 / 40.7	<b>99.1 / 40.4</b>	98.4 / 30.9
Leather	98.8 / 34.1	98.7 / 31.9	<b>98.9 / 35.6</b>	<b>99.6 / 59.3</b>	99.0 / 35.9	<b>99.7 / 61.1</b>	99.0 / 38.5	<b>99.7 / 66.0</b>	98.5 / 29.0
Tile	91.8 / 44.3	<b>99.2 / 57.3</b>	<b>99.3 / 61.5</b>	96.7 / 64.4	<b>96.9 / 65.3</b>	<b>98.0 / 68.1</b>	96.0 / 49.8	<b>98.4 / 76.1</b>	96.8 / 70.2
Wood	<b>93.2 / 37.9</b>	91.5 / 36.7	92.9 / 41.7	<b>96.7 / 59.3</b>	93.3 / 36.2	<b>96.9 / 61.2</b>	92.3 / 48.8	<b>97.2 / 60.4</b>	94.9 / 44.6
Bottle	99.7 / <b>68.2</b>	97.3 / 58.6	97.7 / 59.4	97.4 / 64.7	<b>97.9 / 66.6</b>	<b>98.8 / 76.0</b>	97.9 / 65.3	<b>99.0 / 80.1</b>	98.2 / 70.6
Capsule	98.5 / 47.0	97.7 / 34.6	<b>98.7 / 38.8</b>	96.9 / 26.9	<b>98.5 / 39.9</b>	97.4 / 35.3	<b>98.7 / 39.9</b>	97.8 / 40.7	<b>99.0 / 50.9</b>
Pill	95.0 / 40.9	96.5 / 72.6	<b>97.2 / 74.6</b>	95.1 / 38.4	<b>97.2 / 77.4</b>	95.6 / 43.0	<b>98.8 / 76.4</b>	98.6 / 74.5	<b>98.9 / 85.4</b>
Transistor	<b>97.9 / 73.4</b>	93.7 / 55.2	95.5 / 59.9	83.3 / 28.2	<b>95.0 / 56.7</b>	92.0 / 35.3	<b>97.6 / 66.2</b>	90.2 / 35.0	<b>97.0 / 60.3</b>
Zipper	96.8 / 33.3	97.7 / <b>58.0</b>	<b>98.0 / 56.0</b>	<b>98.5 / 56.2</b>	98.3 / <b>61.8</b>	<b>99.0 / 71.0</b>	98.1 / 68.8	<b>99.2 / 70.2</b>	<b>99.2 / 73.4</b>
Cable	<b>97.3 / 53.2</b>	96.3 / 30.5	96.9 / 48.7	85.4 / 31.7	<b>96.6 / 47.1</b>	92.5 / 42.2	<b>97.4 / 49.9</b>	92.0 / 38.1	<b>98.1 / 56.4</b>
Hazelnut	98.1 / <b>53.8</b>	<b>98.2 / 50.9</b>	<b>98.2 / 51.2</b>	97.8 / <b>62.7</b>	<b>98.2 / 52.3</b>	98.1 / <b>62.1</b>	<b>98.7 / 57.9</b>	98.6 / <b>62.9</b>	<b>98.7 / 60.3</b>
Metal_mnt	94.8 / 49.5	97.4 / 81.3	<b>98.1 / 85.1</b>	96.4 / 61.7	<b>98.7 / 91.8</b>	97.4 / 76.6	<b>98.7 / 90.8</b>	98.2 / 71.6	<b>98.9 / 95.6</b>
Screw	<b>98.3 / 25.0</b>	95.9 / 18.0	97.4 / 23.8	<b>98.6 / 32.5</b>	98.1 / 23.4	98.7 / <b>30.1</b>	<b>98.8 / 27.8</b>	98.5 / 30.5	<b>99.1 / 30.8</b>
Toothbrush	<b>98.4 / 39.4</b>	98.1 / 53.6	98.2 / <b>54.3</b>	97.1 / 33.8	<b>98.5 / 60.9</b>	97.8 / 33.5	<b>98.7 / 52.8</b>	<b>98.9 / 50.1</b>	<b>98.9 / 50.6</b>
<b>MVTec-AD</b>	96.8 / 44.9	96.5 / 48.0	97.2 / <b>50.6</b>	95.8 / 48.6	<b>97.5 / 53.8</b>	97.3 / 53.9	<b>97.7 / 56.4</b>	97.6 / 58.1	<b>98.2 / 58.7</b>
Candle	<b>99.2 / 6.30</b>	98.6 / <b>14.4</b>	97.6 / 11.7	<b>99.5 / 19.7</b>	98.2 / 12.8	<b>99.6 / 25.7</b>	99.3 / 12.4	<b>99.7 / 30.1</b>	98.3 / 18.8
Capsules	84.3 / 0.30	<b>97.1 / 15.1</b>	<b>97.1 / 12.8</b>	97.7 / <b>18.4</b>	<b>98.0 / 16.8</b>	<b>98.9 / 50.7</b>	<b>98.9 / 42.7</b>	99.2 / 56.7	<b>99.4 / 59.2</b>
Cashew	99.6 / 54.6	<b>99.7 / 74.3</b>	99.3 / 69.2	95.5 / 21.1	<b>99.7 / 69.9</b>	95.8 / 27.4	<b>99.7 / 69.6</b>	96.3 / 33.7	<b>99.6 / 66.2</b>
Chewinggum	<b>99.2 / 58.3</b>	98.9 / 29.3	98.8 / 31.6	<b>99.9 / 69.4</b>	99.1 / 57.5	<b>99.9 / 80.1</b>	99.2 / 62.6	<b>99.9 / 78.8</b>	99.4 / 66.8
Fryum	<b>98.4 / 35.9</b>	96.9 / 42.6	97.2 / <b>44.2</b>	96.3 / 25.1	<b>97.6 / 48.0</b>	96.7 / 33.4	<b>98.8 / 56.2</b>	97.4 / 41.7	<b>99.1 / 56.2</b>
Macaroni1	<b>98.6 / 0.94</b>	96.9 / 3.80	97.9 / <b>4.40</b>	<b>99.6 / 11.0</b>	99.1 / 5.70	<b>99.7 / 18.1</b>	99.6 / 9.92	<b>99.7 / 17.8</b>	<b>99.7 / 11.8</b>
Macaroni2	93.4 / 0.06	93.6 / 0.23	<b>93.8 / 0.32</b>	<b>98.5 / 3.40</b>	95.8 / 0.60	<b>99.0 / 6.70</b>	96.6 / 1.20	<b>99.1 / 6.60</b>	97.9 / 2.83
Pcbl	<b>99.5 / 42.1</b>	99.2 / 80.9	99.3 / <b>82.3</b>	98.8 / 53.5	<b>99.7 / 73.4</b>	98.7 / 60.6	<b>99.6 / 81.1</b>	99.1 / 83.9	<b>99.7 / 84.1</b>
Pcbl2	<b>98.3 / 4.67</b>	<b>98.3 / 19.1</b>	<b>98.3 / 15.9</b>	95.8 / 19.0	<b>99.0 / 18.1</b>	96.2 / <b>23.2</b>	<b>98.8 / 18.9</b>	96.3 / <b>38.0</b>	<b>99.4 / 29.1</b>
Pcbl3	98.1 / 9.41	98.3 / 12.1	<b>98.8 / 19.8</b>	96.0 / <b>20.7</b>	<b>98.7 / 19.7</b>	96.3 / 30.1	99.0 / 27.3	96.5 / <b>34.9</b>	<b>99.2 / 25.0</b>
Pcbl4	<b>99.0 / 24.7</b>	98.8 / 26.1	97.9 / 25.3	95.9 / 13.2	<b>98.5 / 23.1</b>	98.5 / 41.6	<b>99.7 / 38.3</b>	98.8 / 44.1	<b>99.7 / 43.7</b>
Pipe_fryum	<b>99.7 / 49.5</b>	99.6 / 62.1	99.5 / <b>64.2</b>	98.8 / 36.9	<b>99.6 / 57.4</b>	99.4 / 51.7	<b>99.7 / 63.8</b>	99.5 / 55.4	<b>99.7 / 61.2</b>
<b>VisA</b>	97.3 / 23.9	97.5 / 31.7	<b>98.0 / 31.8</b>	97.7 / 25.9	<b>98.6 / 33.6</b>	98.2 / 37.5	<b>99.0 / 40.3</b>	98.4 / 43.5	<b>99.3 / 43.7</b>

these nonlinear layers. The AdamW [15] optimizer is used, with a learning rate of 0.0001 for the linear layer in the cross-attention and the projection layer, 0.0002 for the MLP. The weight decay for the MLP is set at 1e-5. The training process extends over 48 epochs, with a batch size of 32.

### 4.3 Experiment Protocols

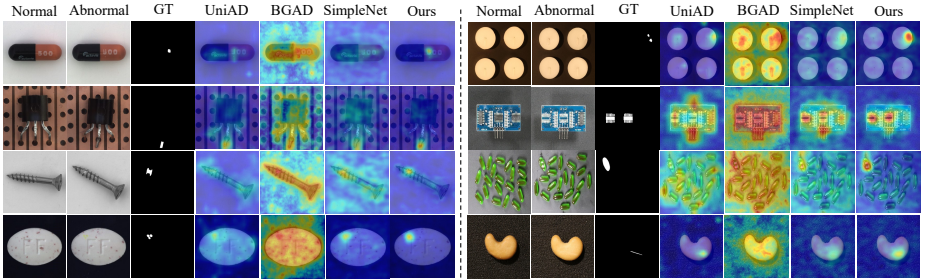
In real-world scenarios, annotated anomalies may or may not be accessible, and the number of anomalies can fluctuate. To evaluate the performance of DMAD in real-world anomaly detection, we examine DMAD in both unsupervised and semi-supervised contexts within a unified setting. The details are as follows:

**Unified Setting (Unsupervised).** This is also known as a multi-class setting. Following [25], the training data consists of normal images from all objects in the dataset, with no anomalies included. The test set contains both normal and abnormal images, and evaluation is conducted separately for each object.

**Unified Semi-Supervised Setting.** This setting is applicable to real-world anomaly detection. To simulate varying quantities of anomalies that could be encountered in real-world scenarios, we set the possible number of accessible annotated anomalies for each object to 1, 5, and 10, respectively. The observed anomalies are randomly selected from each object’s test set and are excluded during evaluation. It should be noted that for the VisA dataset, we directly select anomalies from its training set.

### 4.4 Anomaly Detection and Localization

We conducted a series of both qualitative and quantitative comparison experiments on the MVTec-AD and VisA datasets. The results were subsequently ana-



**Fig. 4:** Qualitative comparison of our method with UniAD [25], BGAD [24] and SimpleNet [14] on MVTec-AD (Left) and VisA (Right) dataset.

lyzed. We selected the benchmark of the unified (multi-class) setting, UniAD [25], a state-of-the-art one-class method, SimpleNet [14], and two semi-supervised methods, DRA [8] and BGAD [24] for comparison. Due to the unavailability of the code for PRN [28], we did not include it in our comparison. Furthermore, we did not present the pixel-level metric of DRA [8], as the code for its anomaly map generation has not been released yet. It should be noted that these methods do not provide results in a unified setting, so we implemented them ourselves, denoted by a \* in the top right corner.

Table 1 and Table 2 presents a quantitative comparison for anomaly detection. In unsupervised scenarios, DMAD, despite not being specifically designed for such situations, demonstrates performance on par with UniAD [25] when tested on the MVTec-AD dataset. Furthermore, it outperforms UniAD [25] on the VisA dataset, achieving gains of 5.8 $\uparrow$  and 42.9 $\uparrow$  in AUROC and AP, respectively. When a few annotated anomalies are available, DMAD utilizes the dual memory bank to learn a more precise decision boundary, thereby achieving state-of-the-art performance on both the MVTec-AD and VisA datasets. Specifically, in a setting with 10 anomalies, DMAD can achieve an AUROC of 99.0 and an AP of 99.7 for anomaly detection in MVTec-AD, and 94.9 AUROC, 79.7 F1max and 84.9 AP in VisA. The anomaly localization performance comparison is shown in Table 2 and Table 3. DMAD achieves the SOTA AUROC/AP/PRO metrics for all different settings, demonstrating its ability to effectively handle the challenges presented by real-world scenarios. More specifically, DMAD achieves up to 98.2 AUROC and 58.7 AP on the MVTec-AD dataset, as well as 99.3 AUROC, 43.7 AP and 92.9 PRO on the VisA dataset.

We also conduct a qualitative evaluation of anomaly localization, as shown in Figure 4. Intuitively, our method facilitates a more accurate identification.



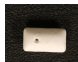

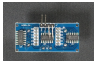

#### 4.5 Ablation Study

To validate the efficacy of the proposed modules, we conducted comprehensive ablation studies on the MVTec-AD dataset, as illustrated in Table 4. Det. and Loc. denote the results of Image-level and Pixel-level AUROC, respectively.

**Table 4:** Ablation study results for our architecture.

	<i>Filter</i>	Dual Memory Bank				Knowledge		Det.	Loc.
		$\mathcal{M}_n$	$\mathcal{M}_a$			<i>dist</i>	<i>Attn</i>		
			$\mathcal{M}_o$	$\mathcal{M}_{a_s}$	$\mathcal{M}_p$				
Unsupervised		✓				✓		94.9	96.0
		✓				✓	✓	95.8	97.1
		✓	✓			✓	✓	<b>96.3</b>	<b>97.2</b>
Semi-supervised		✓	✓	✓		✓		93.6	72.3
	✓	✓	✓	✓		✓		98.7	98.1
	✓	✓	✓	✓		✓	✓	95.4	97.1
	✓	✓	✓	✓	✓	✓		<b>99.0</b>	<b>98.2</b>

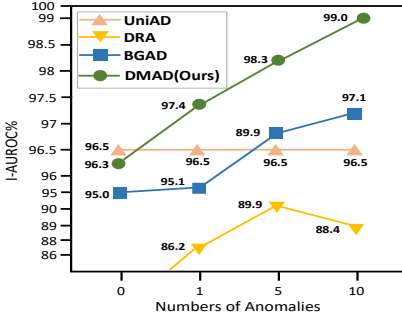
**Table 5:** Quantitative comparison between different scenarios.

Class	Typical Defect	Similar Defect	Setting	Det.	Loc.
macaronil			unsupervised	86.9(+0.0)	97.9(+0.0)
			supervised <sub>others</sub>	91.2(+4.3)	99.2(+1.2)
			supervised	97.3(+10.4)	99.7(+1.7)
chewinggum			unsupervised	97.1(+0.0)	98.8(+0.0)
			supervised <sub>others</sub>	98.6(+1.5)	99.1(+0.3)
			supervised	98.7(+1.6)	99.4(+0.6)
pcb2			unsupervised	94.1(+0.0)	98.3(+0.0)
			supervised <sub>others</sub>	96.7(+2.6)	98.5(+0.2)
			supervised	98.5(+4.4)	99.4(+1.1)

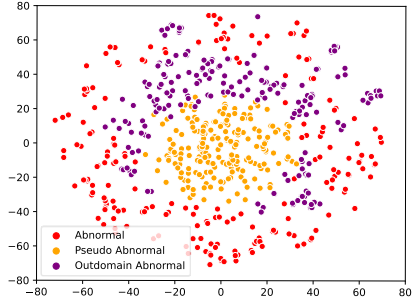
**Knowledge’s Components.** DMAD utilizes a dual memory bank to calculate knowledge related to both normal and abnormal, incorporating a distance *dist* and an attention matrix *Attn*. In unsupervised contexts, we observed that the application of *Attn* boosts performance. Conversely, in semi-supervised contexts, we found that relying exclusively on *dist* as the primary source of knowledge produces superior outcomes. We hypothesize that this discrepancy is attributable to the relatively sparse number of anomalies; an overemphasis on knowledge about these rare anomalies could potentially result in overfitting.

**Abnormal Memory Bank’s Components.** In unsupervised scenarios, no anomalies are available for use. Although a single normal memory bank could also be utilized for anomaly detection, we found that employing a pseudo abnormal memory bank  $\mathcal{M}_o$ , composed of pseudo abnormal features augmented with outlier data, could significantly enhance performance. This approach led to a 0.5 $\uparrow$ /0.1 $\uparrow$  improvement in image-level AUROC and pixel-level AUROC. For semi-supervised scenarios, we proposed an anomaly center sampling strategy to generate an additional pseudo abnormal feature set. The integration of this set resulted in a noticeable enhancement in the model’s performance, leading to a 0.3 $\uparrow$ /0.1 $\uparrow$  improvement in image-level AUROC and pixel-level AUROC.

**Filter Operation.** Introducing anomalies into the framework by directly adding a branch for seen anomalies  $\mathcal{X}_{a_s}$  was ineffective, as anomalous images contain both normal and abnormal regions. Instead, we introduced a selective anomaly filter *Filter*, which significantly improved results.



**Fig. 5:** I-AUROC comparison for varying numbers of anomalies on MVTeC.



**Fig. 6:** Visualization of three different abnormal features in memory bank.

## 4.6 Analysis

**Learning from other object’s defects.** We conducted a specific analysis on the VisA dataset, selected objects include "Macaroni1" (Multiple Instances), and "Chewinggum" and "Pcb2" (Single Instance), to investigate if the seen anomalies from other object could enhance the performance of the target object. The results are detailed in Table 5. Det. and Loc. represent the results of Image-level and Pixel-level AUROC, respectively. Any gains are highlighted in **red**. The setting include no anomalies used (unsupervised), anomalies used (supervised), and anomalies from other objects used (supervised<sub>others</sub>). We consider the **unsupervised** setting as the baseline. Initially, we introduced seen anomalies from all other classes, excluding the anomalies of the class itself for training, denoted as supervised<sub>others</sub>, resulted in a performance boost for each class. This finding suggests that under the unified semi-supervised setting, similar defects across different objects can be beneficial, thereby validating our hypothesis and underscoring the importance of this setting. Furthermore, when we introduced the supervision information of the class itself (*i.e.* **supervised**), we observed additional performance improvements.

**Real-world Anomaly Detection.** A unified model is more practical for real-world anomaly detection, and in real-world scenes, the number of anomalies could be varied. DMAD could handle both unsupervised and semi-supervised scenarios and is benefits of growing anomalies, which is shown in Figure 5.

**Intuitively visualization of Abnormal Memory Bank.** DMAD use a three parts feature to comprised the abnormal memory bank, the outlier data augmented features, seen abnormal features, and the pseudo abnormal features generated by anomaly center sampling strategy. We use t-SNE to reduction the three anomaly features, which is shown in Figure 6, we could see the new anomalies greatly enhances the diversity of abnormal.

## 5 Conclusion

In this study, we tackle real-world anomaly detection by introducing a novel framework, which we have named Dual Memory bank enhanced representation

learning for Anomaly Detection (DMAD). DMAD is a unified framework capable of managing both unsupervised and semi-supervised scenarios within a multi-class setting. It employs a dual memory bank to compute the knowledge of normal and abnormal instances, which is then used to construct an enhanced representation for anomaly score learning. Evaluation results on the MVTec-AD and VisA datasets demonstrate the superior performance of DMAD.

**Limitation.** In practical industrial scenarios, the number of anomalies can vary significantly. This study merely simulates simplified scenes, setting the number of anomalies to 0 (unsupervised), 1, 5, and 10. Furthermore, per-pixel annotation for anomalies may not be available, with only the class label known. In such cases, a new approach needs to be employed to utilize these anomalies.

**Acknowledgements.** This work was supported by National Science and Technology Major Project (No. 2022ZD0118202), the National Science Fund for Distinguished Young Scholars (No.62025603), the National Natural Science Foundation of China (No. U21B2037, No. U22B2051, No. 62176222, No. 62176223, No. 62176226, No. 62072386, No. 62072387, No. 62072389, No. 62002305 and No. 62272401), and the Natural Science Foundation of Fujian Province of China (No.2021J01002, No.2022J06001).

## References

1. Bergmann, P., Fauser, M., Sattlegger, D., Steger, C.: Mvtec ad—a comprehensive real-world dataset for unsupervised anomaly detection. In: Proceedings of the IEEE/CVF conference on computer vision and pattern recognition. pp. 9592–9600 (2019) [9](#)
2. Bergmann, P., Löwe, S., Fauser, M., Sattlegger, D., Steger, C.: Improving unsupervised defect segmentation by applying structural similarity to autoencoders. arXiv preprint arXiv:1807.02011 (2018) [3](#)
3. Chen, J., Sathe, S., Aggarwal, C., Turaga, D.: Outlier detection with autoencoder ensembles. In: Proceedings of the 2017 SIAM international conference on data mining. pp. 90–98. SIAM (2017) [3](#)
4. Cimpoi, M., Maji, S., Kokkinos, I., Mohamed, S., Vedaldi, A.: Describing textures in the wild. In: Proceedings of the IEEE conference on computer vision and pattern recognition. pp. 3606–3613 (2014) [7](#)
5. Cohen, N., Hoshen, Y.: Sub-image anomaly detection with deep pyramid correspondences. arXiv preprint arXiv:2005.02357 (2020) [3](#)
6. Defard, T., Setkov, A., Loesch, A., Audigier, R.: Padim: a patch distribution modeling framework for anomaly detection and localization. In: ICPR (2021) [1](#), [3](#)
7. Dehaene, D., Frigo, O., Combrexelle, S., Eline, P.: Iterative energy-based projection on a normal data manifold for anomaly localization. arXiv preprint arXiv:2002.03734 (2020) [3](#)
8. Ding, C., Pang, G., Shen, C.: Catching both gray and black swans: Open-set supervised anomaly detection. In: Proceedings of the IEEE/CVF Conference on Computer Vision and Pattern Recognition. pp. 7388–7398 (2022) [2](#), [4](#), [10](#), [12](#)
9. He, H., Zhang, J., Chen, H., Chen, X., Li, Z., Chen, X., Wang, Y., Wang, C., Xie, L.: Diad: A diffusion-based framework for multi-class anomaly detection. In: AAAI (2024) [3](#)



10. Hu, T., Zhang, J., Yi, R., Du, Y., Chen, X., Liu, L., Wang, Y., Wang, C.: Anomalydiffusion: Few-shot anomaly image generation with diffusion model. In: AAAI (2024) [4](#)
11. Li, C.L., Sohn, K., Yoon, J., Pfister, T.: Cutpaste: Self-supervised learning for anomaly detection and localization. In: Proceedings of the IEEE/CVF conference on computer vision and pattern recognition. pp. 9664–9674 (2021) [4](#)
12. Liang, Y., Zhang, J., Zhao, S., Wu, R., Liu, Y., Pan, S.: Omni-frequency channel-selection representations for unsupervised anomaly detection. IEEE Transactions on Image Processing (2023) [3](#)
13. Liu, W., Li, R., Zheng, M., Karanam, S., Wu, Z., Bhanu, B., Radke, R.J., Camps, O.: Towards visually explaining variational autoencoders. In: Proceedings of the IEEE/CVF Conference on Computer Vision and Pattern Recognition. pp. 8642–8651 (2020) [3](#)
14. Liu, Z., Zhou, Y., Xu, Y., Wang, Z.: Simplenet: A simple network for image anomaly detection and localization. In: Proceedings of the IEEE/CVF Conference on Computer Vision and Pattern Recognition. pp. 20402–20411 (2023) [1](#), [4](#), [5](#), [9](#), [10](#), [11](#), [12](#)
15. Loshchilov, I., Hutter, F.: Decoupled weight decay regularization. arXiv preprint arXiv:1711.05101 (2017) [11](#)
16. Pang, G., Ding, C., Shen, C., Hengel, A.v.d.: Explainable deep few-shot anomaly detection with deviation networks. arXiv preprint arXiv:2108.00462 (2021) [2](#)
17. Roth, K., Pemula, L., Zepeda, J., Schölkopf, B., Brox, T., Gehler, P.: Towards total recall in industrial anomaly detection. In: CVPR (2022) [3](#), [6](#), [10](#)
18. Ruff, L., Vandermeulen, R.A., Görnitz, N., Binder, A., Müller, E., Müller, K.R., Kloft, M.: Deep semi-supervised anomaly detection. arXiv preprint arXiv:1906.02694 (2019) [4](#)
19. Sabokrou, M., Khalooei, M., Fathy, M., Adeli, E.: Adversarially learned one-class classifier for novelty detection. In: Proceedings of the IEEE conference on computer vision and pattern recognition. pp. 3379–3388 (2018) [3](#)
20. Schlegl, T., Seeböck, P., Waldstein, S.M., Langs, G., Schmidt-Erfurth, U.: f-anogan: Fast unsupervised anomaly detection with generative adversarial networks. Medical image analysis **54**, 30–44 (2019) [3](#)
21. Schlegl, T., Seeböck, P., Waldstein, S.M., Schmidt-Erfurth, U., Langs, G.: Unsupervised anomaly detection with generative adversarial networks to guide marker discovery. In: International conference on information processing in medical imaging. pp. 146–157. Springer (2017) [3](#)
22. Schlüter, H.M., Tan, J., Hou, B., Kainz, B.: Natural synthetic anomalies for self-supervised anomaly detection and localization. In: European Conference on Computer Vision. pp. 474–489. Springer (2022) [4](#)
23. Wang, Y., Peng, J., Zhang, J., Yi, R., Wang, Y., Wang, C.: Multimodal industrial anomaly detection via hybrid fusion. In: Proceedings of the IEEE/CVF Conference on Computer Vision and Pattern Recognition. pp. 8032–8041 (2023) [1](#)
24. Yao, X., Li, R., Zhang, J., Sun, J., Zhang, C.: Explicit boundary guided semi-push-pull contrastive learning for supervised anomaly detection. In: Proceedings of the IEEE/CVF Conference on Computer Vision and Pattern Recognition. pp. 24490–24499 (2023) [2](#), [4](#), [10](#), [11](#), [12](#)
25. You, Z., Cui, L., Shen, Y., Yang, K., Lu, X., Zheng, Y., Le, X.: A unified model for multi-class anomaly detection. Advances in Neural Information Processing Systems **35**, 4571–4584 (2022) [1](#), [4](#), [5](#), [10](#), [11](#), [12](#)
26. Zagoruyko, S., Komodakis, N.: Wide residual networks. arXiv preprint arXiv:1605.07146 (2016) [10](#)



27. Zavrtnik, V., Kristan, M., Skočaj, D.: Draem-a discriminatively trained reconstruction embedding for surface anomaly detection. In: Proceedings of the IEEE/CVF International Conference on Computer Vision. pp. 8330–8339 (2021) [4](#)
28. Zhang, H., Wu, Z., Wang, Z., Chen, Z., Jiang, Y.G.: Prototypical residual networks for anomaly detection and localization. In: Proceedings of the IEEE/CVF Conference on Computer Vision and Pattern Recognition. pp. 16281–16291 (2023) [2](#), [4](#), [12](#)
29. Zhang, J., Chen, X., Wang, Y., Wang, C., Liu, Y., Li, X., Yang, M.H., Tao, D.: Exploring plain vit reconstruction for multi-class unsupervised anomaly detection. arXiv preprint arXiv:2312.07495 (2023) [3](#)
30. Zhao, Y.: Omnia: A unified cnn framework for unsupervised anomaly localization. In: Proceedings of the IEEE/CVF Conference on Computer Vision and Pattern Recognition. pp. 3924–3933 (2023) [4](#)
31. Zhou, C., Paffenroth, R.C.: Anomaly detection with robust deep autoencoders. In: Proceedings of the 23rd ACM SIGKDD international conference on knowledge discovery and data mining. pp. 665–674 (2017) [1](#), [3](#)
32. Zou, Y., Jeong, J., Pemula, L., Zhang, D., Dabeer, O.: Spot-the-difference self-supervised pre-training for anomaly detection and segmentation. In: European Conference on Computer Vision. pp. 392–408. Springer (2022) [9](#)